THE EFFECT OF MAGNESIUM ON THE FORMATION OF CaCO₃ DEPOSITIONS

E. Puhakka[1], M. Riihimäki[2] and R.L. Keiski[2]

[1] VTT Technical Research Centre of Finland, P.O. Box 1000, FI-02044 VTT, Finland and E-mail: eini.puhakka@vtt.fi
[2] University of Oulu, Mass and Heat Transfer Process Laboratory, P.O. Box 4300, FI-90014 University of Oulu, Finland

ABSTRACT

In decreasing the carbon footprint of process industry, the controlling of energy efficiency of process equipment has a significant role. One of the most marked factors in improving the energy efficiency is the mitigation of precipitation and crystallization onto the heat transfer surfaces. In many cases, analysis of deposited materials reveals that the trace compounds of process fluids are concentrated onto surfaces. Thus, trace compounds can affect fouling rate, structure and morphology of deposited materials and adhesion strength of depositions on the surfaces. In this study, formation of CaCO₃ depositions in the presence of magnesium ions was investigated on stainless steel surfaces at the laboratory scale conditions. Deposition formation was also studied using molecular modelling methods in order to clarify the detailed formation mechanisms. In addition to stainless steel, diamond and zirconium nitride coatings were considered with modelling methods. The aim of the study was to clarify the effect of magnesium on the crystallization fouling. This work consisted of both molecular modelling research and experimental fouling experiments at the laboratory scale in order to clarify the detailed mechanisms for the deposition formation.

INTRODUCTION

Fouling of heat transfer surfaces is a marked problem which reduces the thermal efficiency of heat transfer units and which is one of the major unresolved problems in most industrial processes (Bott, 1997). It causes economical losses and challenging problems to overcome in actual processes, and globally fouling has the marked effect on carbon dioxide releases and on climate change. It is estimated that fouling costs are about 0.2% of the countries' Gross National Product (Müller-Steinhagen, 2002).

In industrial processes, depositions of inversely soluble cationic salts, like calcium carbonate (CaCO₃), are rather typical depositions, which form unwanted depositions with trace compounds as magnesium and silicon onto heat transfer surfaces. Since CaCO₃ is inversely soluble in water, the water-soluble calcium loses its ability to remain in solution and precipitates as a hard solid on heated surfaces. This inverse solubility behavior allows the salt to form an insulating deposit on the heat transfer surfaces. The deposit will then obstruct heat transfer, which leads to energy wastage and inhibition of fluid flow. Though, depositions are typically cleanable with acids, still costs of energy losses, operation and maintenance are significant. Because prevention of calcium depositions is difficult by controlling process conditions, new novel techniques are on development. For example, new surface materials can be useful in order to mitigate fouling in industrial processes.

A prerequisite for a development of materials is that the adhesion mechanisms of depositions onto surfaces are known. Fouling mechanisms can be classified into six groups: crystallization, particle attachment, chemical fouling, corrosion, biological fouling and solidification (Bott, 1995; Mwaba et al., 2006). The fouling rate, the chemical composition and the physical properties of deposited material on the surfaces depend on process conditions (e.g. pH, temperature, concentrations of soluble species of particles, fluid flow) and construction materials of heat transfer surfaces (Kostoglou and Karabelas, 1998). When the deposition formation of inversely soluble CaCO₃ will be considered, the role of crystallization fouling is the most probable mechanism in the initiation of the fouling. Further, the crystallization fouling caused by CaCO₃ solutions is very harmful in several industrial processes e.g. in dewatering and evaporation processes.

Because it is very demanding to gather information about interaction mechanisms (chemical or physical nature of bonding) between heat transfer surfaces and depositions with experimental methods, we utilized both laboratory scale fouling experiments and molecular modelling in order to obtain explanations for the attachment of depositions at the molecular level (Puhakka et al., 2011; Pääkkönen et al., 2010). The initiation mechanism of crystallization fouling was determined on the silicon dioxide (SiO₂), diamond and titanium carbide (TiC) surfaces at the molecular level. Experimental tests and analyses of depositions gave qualitative and quantitative information on the bulk properties and composition of depositions. Now, the role of trace compounds, like magnesium and silicates, on the deposition formation was investigated. The trace compounds can affect fouling rate, structure and morphology of deposited materials and adhesion strength of depositions on the surfaces.

The aim of this study was to clarify, if it is possible to use diamond like carbon (DLC) and zirconium nitride (ZrN) coatings instead of pure stainless steel surface in order to avoid CaCO₃ depositions. In the molecular modelling studies, the original X-Ray diffraction (XRD)

structure was utilized in order to describe the surface structures of ZrN, but for stainless steel and DLC, the simplified structures of the materials were used.

The properties of stainless steel are based on the passive layer on the surface, which mainly consists of chromium oxides and has a thickness of about ten molecular layers (Pießlinger-Schweiger, 2005). Therefore, the passive layer of stainless steel was described with the hexagonal dichromium trioxide (Cr_2O_3) structure. The DLC coating is mainly amorphous, but XRD analyses for the DLC coatings on stainless steel substrates have indicated that there is also a crystalline phase on the surface structure of DLC coatings (Puhakka et al., 2011). Based on this detection, the surface structure of DLC was described using the structure of diamond. The surface roughness cannot be taken into account in these modelling studies.

The investigated coatings were selected based on industrial interest, when fouling caused by inversely soluble salts, like $CaCO_3$, in the presence of trace compounds is attempted to mitigate on heat transfer surfaces. The effect of trace compounds (copper, iron and zinc) on calcite nucleation and precipitation has also been investigated earlier (Macadem and Parsons, 2004). It was detected that $CaCO_3$ depositions are sensitive to impurity ions, and the most effective inhibitor of $CaCO_3$ precipitation is zinc, and copper and iron has only little effect. Investigation on fouling behaviours of low-energy copper-modified surfaces has indicated that the fouling is enhanced in the presence of desorbed air bubbles on the modfied surfaces (Yang et al., 2000). Further, it is detected that fouling resistance can be reduced only during induction period owing to the weaker adhesion strength of fouling (Yang et al., 2000).

In this study, the focus has been on the effect of magnesium (Mg^{2+}) on the formation of $CaCO_3$ depositions. Generally, it is known that magnesium has an inhibiting effect on the growth of calcite (the most stable polymorph of $CaCO_3$) in the aqueous solution (Astilleros et al., 2010; Chen et al., 2005; Chen et al., 2006; Nishino et al., 2009). It is presumable that magnesium (Mg^{2+}) suppresses the growth of calcite crystals, because Mg^{2+} incorporates into the calcite structure, which is supposed to be more soluble than the pure calcite phase. On the other hand, the lateral crystal growth (c-axis) is prevented in the presence of Mg^{2+} ions, because Mg^{2+} as a smaller than calcium (Ca^{2+}) causes distortions for the calcite lattice. Of formed particles in bulk fluid, aragonite particles are more adherent and enhance deposition formation compared to calcite particles (Andritsos and Karabelas, 2003).

METHODS

Molecular Modelling

Density functional methods were used to investigate the crystal and surface structures of stainless steel and coating materials. The investigated coatings were diamond and ZrN. Because surfaces are subject to the effect of ambient process conditions, the role of process fluid (water) for surface structures was taken into account. Therefore, the adsorption mechanism of water onto the surfaces was investigated, and the model surfaces for deposition formation studies were generated. These surfaces were used to study the adsorption of magnesium (Mg^{2+}), and carbonate (CO_3^{2-}) ions onto surfaces, and the formation mechanism of carbonate depositions. All the calculations were performed with the CASTEP (CAmbridge Serial Total Energy Package) code implemented into Materials Studio versions 4.1 (Accelrys, 2006), 4.2 (Accelrys, 2007), 4.3 (Accelrys, 2008a), 4.3.1 (Accelrys, 2008b) and 5.0 (Accelrys, 2009). In these calculations, the total electronic energy and overall electronic density distribution were solved in order to define the energetically stable structures for surfaces and adsorbates on the surfaces (Leach, 2001).

During the geometry optimization of the crystal and surface structures of coatings, and adsorption studies of water and Mg^{2+} and CO_3^{2-} ions onto the surfaces, the exchange-correlation was described with generalized gradient approximation GGA-PBE. As a compromise between the accuracy and computational time of calculations, the ultrasoft pseudopotentials were used for each element. In the potential of chromium, the semicore states were treated as a part of the core. The used potentials were C_00PBE.usp for carbon, Cr_00PBE.uspcc for chromium, H_00.usp for hydrogen, Mg_00.usp for magnesium, N_00PBE.usp for nitrogen, O_soft00.usp for oxygen, and Zr_00PBE.usp for zirconium. The kinetic cut-off energy for a plane wave expansion of the wave function was 280 eV, except for structures containing Mg^{2+}, cut-off energy was 310 eV. The morphology of coatings was predicted by using the BFDH (Bravais-Friedel Donnay-Harker) method.

Energy values for the formation of $MgCO_3$ depositions were calculated from the single-point energies of the ions and the surface structures with and without the adsorbed ions. The calculations were performed using the GGA-RPBE exchange-correlation, and the kinetic cut-off energy was 330 eV.

Experimental Set-up

Experiments were performed with the laboratory test facility described in Riihimäki et al. (2010). The set-up was the one described in Pääkkönen et al. (2010). This set-up consisted of two stainless steel (AISI 316L) flat plate test sections, size of 0.1 m x 0.2 m, in rectangular flow channel which flow area was 0.1 m x 0.015 m. Steel plates were heated by ohmic heaters (2 x 102 Ω) that were connected to a power transmitter (Powernet DC7480/220AI 3200W) to get constant, but adjustable heat flux.

Test Fluid

The test solution, which was prepared by mixing $CaCl_2 \cdot 2H_2O$, $NaHCO_3$, and $MgCl_2 \cdot 6H_2O$ (BDH Prolabo) salts to the deionized water, was circulated to the test section from a mixing tank (100 dm^3). Filters in series (Watman washable nylon 60 μm and Watman polypropene 1 μm) were used before the test section to remove bulk particles from the test solution when necessary. Conductivity of the solution was controlled by dosing conductivity control solution (1.5 g/l $CaCl_2 \cdot 2H_2O$ and 1.5

g/l NaHCO$_3$) automatically to the mixing tank. The conductivity control was used to maintain the concentration level at the test loop approximately constant, and thus to replace the decrease of the ions due to crystallization of the salts.

Experimental Procedure

In every experiment, the mixing tank was first filled with deionized water. After that, the water was heated up to a desired temperature by circulating it in the set-up while the power to the test section and tank heaters was on. Each salt was dissolved to 10 dm^3 amount of heated deionized water and added to the mixing tank in an order CaCl$_2$, NaHCO$_3$ and last MgCl$_2$. A test was started when the surface and inlet temperatures and conductivity measurements were stabilized, not later than five minutes from the addition of the first salt.

The fouling experiments were done in velocity of 0.20 m/s having Reynolds number of 5 200. Thus, the flow was in the transient between laminar and fully turbulent flow regime. Heat fluxes of 68 and 51 kW/m^2 were used in the tests without filters and only 51 kW/m^2 with filters was used. The experiments were done with constant bulk fluid temperature (30 °C). Previously Pääkkönen et al. (2010) studied the effect of velocity and heat flux on fouling of CaCO$_3$ with the fluid used also in this study.

In the experiments without filters, bulk precipitation takes place simultaneously with surface crystallization and effect of magnesium on bulk precipitation was studied. When the effect of magnesium on surface growth was studied, tests were done using filters.

RESULTS AND DISCUSSION

Crystal Structure of the Materials

Fouling properties of different materials depend on the atomic layered structure of material surfaces. In order to investigate the surface structures, the crystal structures of materials have to be known. The chromium-rich oxide layer of stainless steel was described by the hexagonal Cr$_2$O$_3$ (a = b = 495.9 pm, c = 1359.3 pm and c/a = 2.741) with symmetry R-3c (Accelrys 2004). Other crystal structures were cubic diamond (a = b = c = 355.6 pm) and ZrN (a = b = c = 458.5 pm) with symmetry Fd-3m and Fm-3m, respectively (Accelrys, 2006).

In order to perform molecular modelling studies, the calculated lattice parameters for Cr$_2$O$_3$, diamond and ZrN have to be available. The target was that the calculated and experimental lattice parameters are comparable so that the modelling results can be utilized in order to interpret experimental findings. In this study, the earlier calculated lattice parameters for Cr$_2$O$_3$ and diamond were utilized, which are a = b = 513.8 pm, c = 1403.6 pm and c/a = 2.732 for energetically stable Cr$_2$O$_3$ (Puhakka et al., 2008), and a = b = c = 357.4 pm for diamond (Puhakka et al., 2011). New calculated lattice parameters for ZrN were a = b = c = 461.2 pm. These values indicated that the correspondence between the calculated and experimental parameters is good enough, 0.5–3.6%.

Surface Structures

Based on the optimized crystal structures, the most typical surface structures of the materials were predicted by the BFDH method. This theoretical prediction completed the data obtained from XRD measurements of the same structures. According to the BFDH prediction, there are three dominant surfaces, (10-2), (104) and (006) for Cr$_2$O$_3$ (Puhakka et al., 2008), one dominant surface, (111), for diamond (Puhakka et al., 2011), and two dominant surfaces, (111) and (200), for ZrN.

When the role of the dominating crystal planes are considered from a point of view of deposition formation at the molecular level, it is important to notice that the so-called growth planes of materials are not necessarily the planes detected on the surfaces of equipment. Especially, this was significant in the case of Cr$_2$O$_3$, which is the corrosion protective layer of stainless steel. There a fully oxidated (004) surface is more relevant than (10-2), (104) and (006) surfaces where chromium atoms are five- or three-coordinated (Puhakka et al., 2008).

In the case of diamond and ZrN, the (111) surface was selected to advanced studies. For ZrN, the (111) surface is the most dominant crystal plane, where only Zr atoms exist on the top layer of surface. This surface was supposed to be active for surface reaction forming deposition formation. However, it was not taken into account possible oxidation reaction of ZrN into ZrO$_2$. It is known that fully thermally oxidation happens, when temperature is raised to 550 °C (Milošev et al., 1997). Because in our experimental studies, the highest initial wall temperature was 80.2 °C, it was supposed that oxidation does not occur on these surfaces.

In the case of diamond, the deposition conditions of coating were taken into account in order to get a more profound description of the sterical and electrostatic factors of the surface. When the DLC coating is deposited by plasma enhanced chemical vapour deposition (PECVD) and physical vapour deposition (PVD) techniques, hydrogen layer exist on the top-most carbon layer (Grill, 1999; Laikhtman et al., 2004). Hydrogen gives the "diamond-like" properties for materials. Therefore, the cleaved (111) surface covered by hydrogen atoms was used in order to describe the real surface structure as precisely as possible (Puhakka et al., 2011).

Deposition Formation on the Surfaces

When the surface structures were available, then deposition formation studies were started. In this study, the initiation of crystallization fouling caused by Mg^{2+} and CO$_3^{2-}$ species, and water as a process liquor was investigated. It was supposed that water adsorbs firstly onto surfaces, and after that the other species.

The adsorption mechanism of water depends on the surface structure and chemical composition of surfaces. Water can adsorb onto solid surfaces as a molecule, or it can dissociate forming partially or fully hydroxylated surfaces (Cappus et al., 1993; Maurice et al., 2001; Henderson et al., 2000; Henderson, 2002; Saunders et al., 2008; Ignatchenko et al., 2006). Therefore, the type of

adsorption was defined for the (004) surface of Cr_2O_3, the hydrogen-covered (111) surface of diamond and the (111) surface of ZrN, which were used in our study. In order to study the adsorption mechanism, the surfaces were covered by water molecules or hydroxyl groups and protons (dissociated water molecule), and the modified surface structure was allowed to relax in order to receive the stable surface structures.
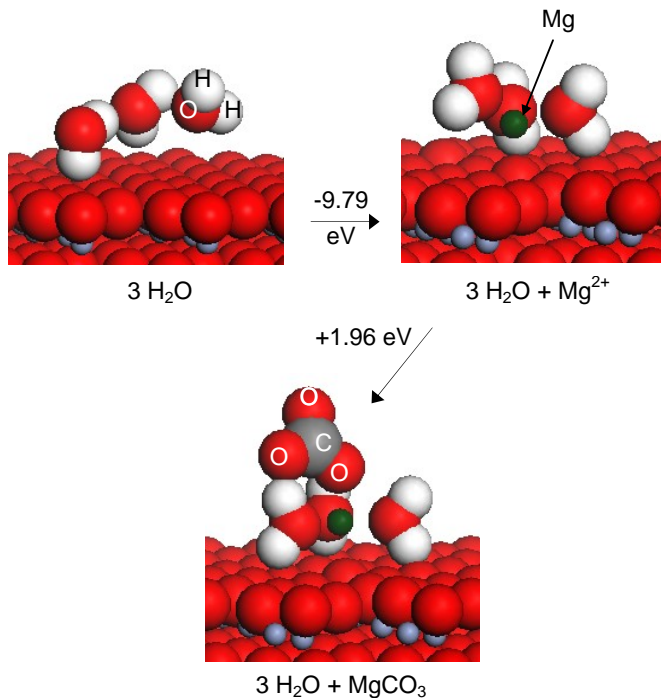
deposition in the next step in the presence of a CO_3^{2-} ion. An additional water on the surface does not affect the structure of deposition. The total energy for this reaction is -8.06 eV.
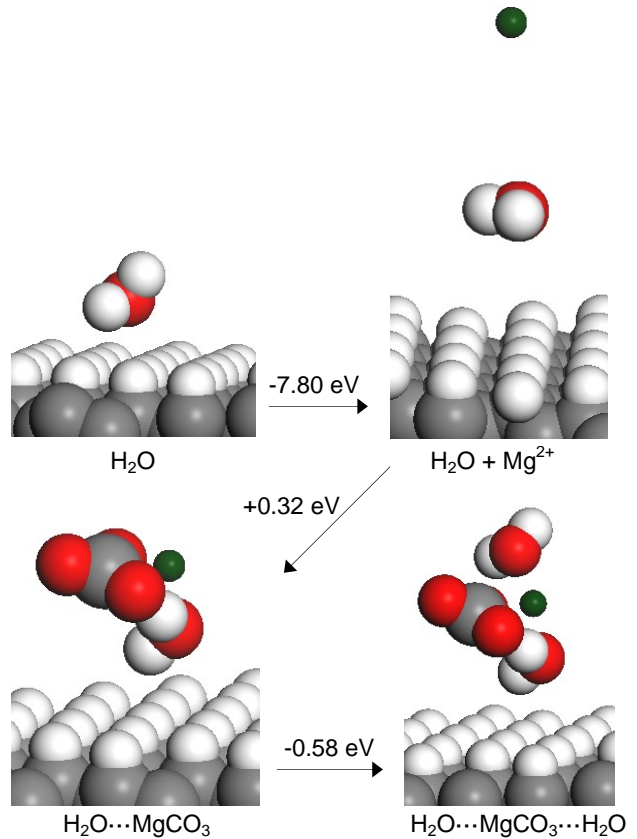

Fig. 1   Formation of $MgCO_3$ deposition on the fully oxidized (004) surface of Cr_2O_3 where the top layer consists of only oxygen atoms. Red spheres: oxygen. Small blue spheres between the oxygen layers: chromium. White spheres: hydrogen. Green spheres: magnesium. Grey sphere: carbon.

Fig. 2   Formation of $MgCO_3$ deposition on the (111) surface of diamond, where the uppermost layer consists of hydrogen. Grey spheres: carbon. White spheres: hydrogen. Green spheres: magnesium. Red spheres: oxygen.

Based on our earlier study (Puhakka et al., 2008), the dissociative adsorption of water is possible onto Cr_2O_3 surfaces. Then, the surfaces would be covered by surface hydroxyl groups. However, energetically it is more presumable that water does not dissociate, but it forms layered water molecule structures onto the surfaces. In the presence of Ca^{2+} ions, the layered water molecules reorientate on the surface forming $Ca^{2+}–(H_2O)_3$ complexes (Puhakka et al., 2011). The same phenomena was also detected in the case of Mg^{2+} ions. The formation mechanism for $MgCO_3$ deposition on the (004) surface of Cr_2O_3 is presented step by step in the Fig. 1. A Mg^{2+} ion adsorbs onto the water-covered surface, and after that a CO_3^{2-} ion adsorbs forming the final deposition. The formation energy of this reaction is -7.83 eV.

On the (111) surface of diamond, dissociation of water does not happen, when the adsorbated hydrogen layer exists on the surface (Fig. 2). In the first step, a Mg^{2+} ion approaches the surface, but it reaches a stable energy level at the height of 1020 pm above the surface. The Mg^{2+} forms

On the (111) surface of ZrN, the dissociation of water is possible, but only half of molecules dissociate (Fig. 3). The energy released in this reaction is -3.28 eV. However, in the presence of Mg^{2+} ions, it is preferable that Mg^{2+} ion adsorbs onto the water-covered surface (Fig. 4), and the adsorption energy is -10.35 eV. The total energy for the deposition formation is -8.44 eV.
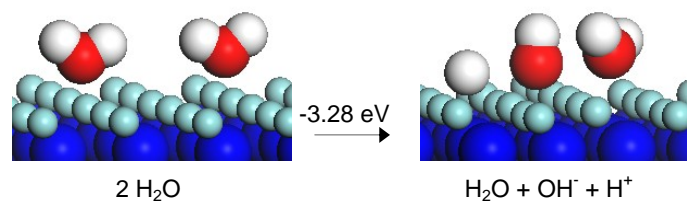

Fig. 3   Dissociation of water on the (111) surface of ZrN. Small light blue spheres: zirconium. Big blue spheres: nitrogen. Red spheres: oxygen. White spheres: hydrogen.

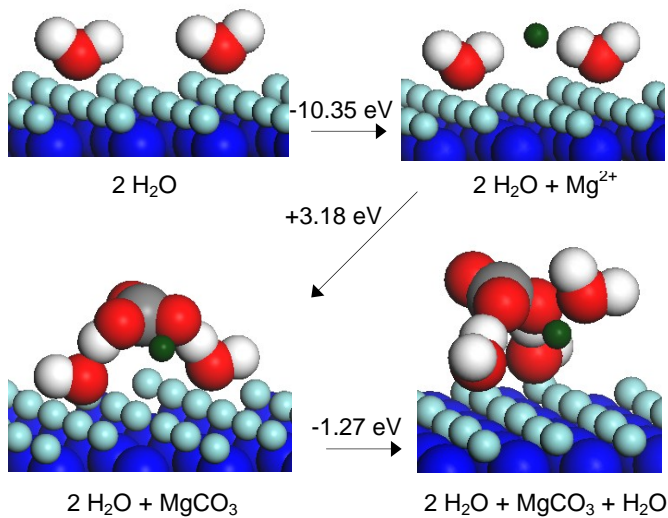2 H$_2$O   −10.35 eV   2 H$_2$O + Mg^{2+}

+3.18 eV

2 H$_2$O + MgCO$_3$ −1.27 eV   2 H$_2$O + MgCO$_3$ + H$_2$O

Fig. 4 Formation of MgCO$_3$ deposition on the (111) surface of ZrN. Small light blue spheres: zirconium. Big blue spheres: nitrogen. Red spheres: oxygen. White spheres: hydrogen. Green spheres: magnesium. Grey spheres: carbon.

Table 1. Formation energies of CaCO$_3$ and MgCO$_3$ depositions.

	Formation energies	
	CaCO$_3$	MgCO$_3$
Cr$_2$O$_3$	-3.15	-7.83
Diamond	-3.31	-8.06
ZrN	-8.01	-8.44

When these results were compared to the earlier calculated results in Table 1 for CaCO$_3$ deposition formation (Puhakka et al., 2011), it was realized that the formation energies of MgCO$_3$ depositions are more exothermic than those of CaCO$_3$ depositions. Based on this, the MgCO$_3$ depositions attach more tightly onto surfaces. It is presumable that this explains the inhibiting effect of Mg^{2+} on the growth of calcite crystals in the aqueous solution (Astilleros et al., 2010; Nishino et al., 2009).

These calculated formation energies correlate with the experimentally determined induction times for crystallization fouling (Puhakka et al., 2010). Because detailed description of the relationship behind the induction time of crystallization is complex and not known, the effect of magnesium on the crystallization fouling was also investigated experimentally.
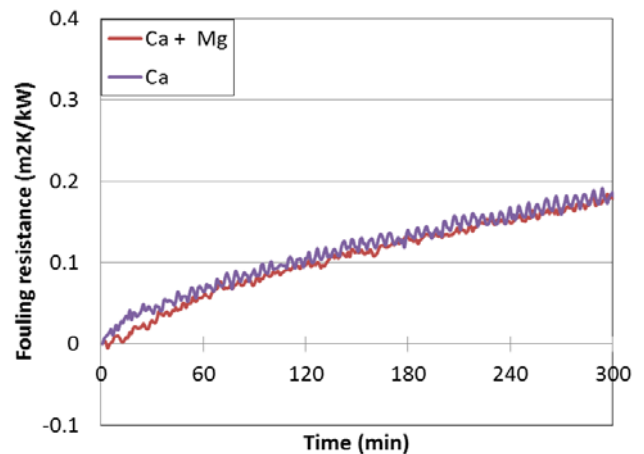
Fouling Experiments

The deposition formation of CaCO$_3$ in presence of Mg^{2+} was investigated in the laboratory scale fouling test apparatus. The effect of magnesium on bulk crystallization and on surface crystallization was studied. The conditions for the tests were selected according to the observations of Pääkkönen et al. (2010) so that there are conditions where bulk precipitation is strong and the formed particles are not

filtered from fluid, and weaker when decreasing concentration and eliminated with using filters.

Fig. 5 presents experiments without filters where the bulk precipitation is (a) strong and (b) weak, while surface growth is still taking place. In Fig. 5a, concentrations of CaCl$_2$·2H$_2$O and NaHCO$_3$ were both equally 0.75 g/l, and 0.75 g/l also for MgCl$_2$·6H$_2$O when it was added, heat flux was 68 kW/m^2, initial wall temperature was 80.2 °C. In Fig. 5b, the concentration of salts were decreased to 0.5 g/l and heat flux to 51 kW/m^2 resulting the initial wall temperature of 68.8 °C. The tests in Fig. 5 showed similar fouling behaviour with and without magnesium addition: induction time was not observed and the fouling rate was practically the same.
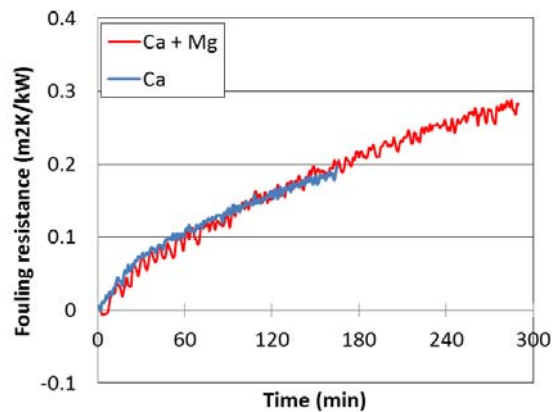
a) Concentrations of salts 0.75 g/l, heat flux 68 kW/m^2, fluid temperature 30 °C, velocity 0.2 m/s.

b) Concentrations of salts 0.5 g/l, heat flux 51 kW/m^2, fluid temperature 30 °C, velocity 0.2 m/s.

Fig. 5 Effect of magnesium on fouling in the tests without filters when bulk precipitation is taking place.

Fig. 6 presents experiments with filters where the deposition of bulk precipitated particles was eliminated and surface growth of crystals dominates fouling. These experiments showed that magnesium has the effect on induction time and deposition rate. The induction time

decreases from 150 min (0 g/l $MgCl_2 \cdot 2H_2O$) to 30 min (0.05 g/l) and further disappears (0.15 g/l). This may indicate that Mg^{2+} shortens so called induction time, the time during stable nucleus of the crystal forms that allows further growth of the crystals. The effect of Mg^{2+} on fouling resistance growth rate is not as clear than the effect on induction time. However, linear fouling resistance growth rates were determined excluding the 300 min from the beginning of the tests. Non-linear part (0-300 min) is due to initiation period when the surface may not be yet fully covered by deposit and surface effects may dominate deposition. During steady fouling period (300-1200 min) rates were $16 \cdot 10^{-7}$ (0 g/l $MgCl_2 \cdot 2H_2O$), $8.3 \cdot 10^{-7}$ (0.05 g/l $MgCl_2 \cdot 2H_2O$) and $10 \cdot 10^{-7}$ $m^2 K/kJ$ (0.15 g/l $MgCl_2 \cdot 2H_2O$). This indicates that Mg^{2+} may have possibility to inhibit crystallization of calcite during steady fouling phase of the deposition.
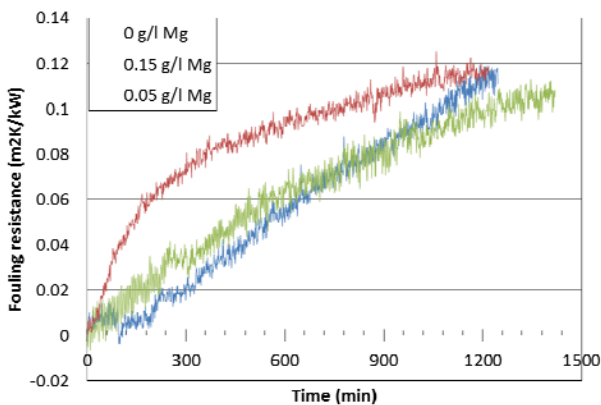

Fig. 6 Fouling curves for the test with filters. Concentration of $NaHCO_3$ and $CaCl_2 \cdot 2H_2O$ was 0.5 g/l, $MgCl_2 \cdot 6H_2O$ 0, 0.05 and 0.15 g/l, fluid temperature 30 °C, velocity 0.2 m/s and heat flux 51 kW/m^2.

Fig. 7 shows the shape of the crystals obtained from the deposited material. When bulk crystallization is strong (a), the deposited material has mostly rhombohedral shaped particles with equal edge lengths, but also some needle shape long orthorhombic crystals are present. At lower concentrations and with added magnesium salt (b), the bulk crystallization is simultaneous with surface crystal growth, and needle shape particles are present in larger amounts. Particle shape seemed to change so that orthorhombic needles get new crystal planes when magnesium is present in the solution. When filters were used (c), mostly needles were forming. It was observed that with magnesium salt addition new crystal planes were forming so that the obtuse angles in orthorhombic crystals disappeared. Formed morphology remained unsymmetrical hexagonal morphology where new edge lengths are shorter than in the symmetrical morphology.

XRD studies showed that orthorhombic aragonite was the main phase in the deposited material. Without magnesium addition, depositions contained orthorhombic aragonite more than 95% of the material and rhombohedral calcite less than 5%. In the experiment without filters

having 0.5 g/l magnesium salt, deposition contained 74% orthorhombic aragonite, 24% rhombohedral magnesium calcite ($Mg_{0.23}Ca_{0.77}CO_3$) and less than 2% rhombhedral dolomite $MgCa(CO_3)_2$.
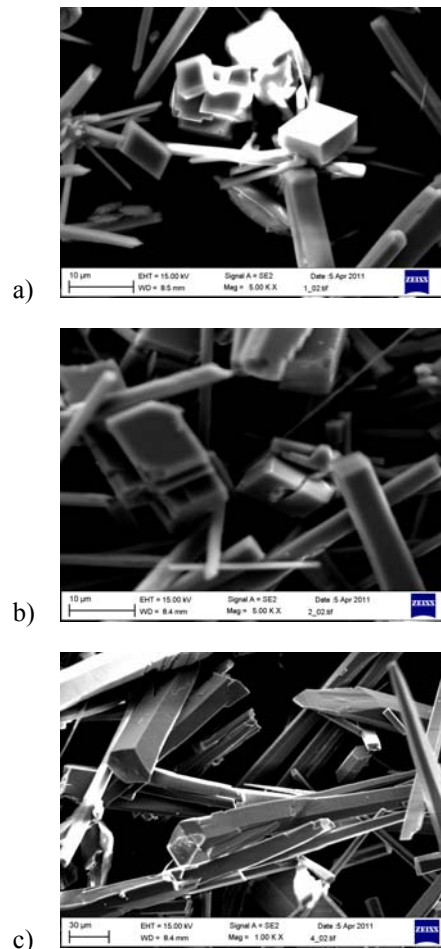

Fig. 7 Crystal shape in different test conditions. (a) strong bulk precipitation (0.75 g/l), (b) weaker bulk precipitation (0.5 g/l) and magnesium salt added (0.5g/l), (c) surface growth when filter used (0.5 g/l) and magnesium salt added (0.5 g/l).

When magnesium is present in the solution, it can replace calcium atoms incorporating Mg^{2+} in to growing crystal lattice whose composition can consequently be described as $Mg_xCa_{1-x}CO_3$. Astilleros et al. (2010) observed growth of calcite {10-14} surface and concluded that the rate at which this advances significantly decreases which is inhibiting calcite growth. Nishino et al. (2009) observed that magnesium would favour the formation of amorphous $CaCO_3$ growth forming spherical particles instead of orthorhombic crystals. According to the experiments of this study in the conditions of heat exchanger with stainless steel (AISI 316) surface did not confirm the observation of inhibition of calcite growth rate and increased induction time. The conditions in heat exchanger differed from the most studies done at room temperature without constant fluid flow. Morphological studies with scanning electron microscopy (SEM) and structural studies with XRD gave

indication of changes in deposited material affected by magnesium that may have the strong effect on the fouling rate and on the induction of crystal growth on heat exchanger surfaces in different conditions both at laboratory scale and in industrial applications.

CONCLUSIONS

Formation of $MgCO_3$ depositions on different surfaces were studied using molecular modelling methods and performing fouling experiments in the laboratory scale. The initiation mechanism of crystallization fouling was determined on the stainless steel, diamond and ZrN surfaces at the molecular level, and the results were compared to the mechanisms of $CaCO_3$ formation. Based on the molecular modelling results, the $MgCO_3$ deposition formation is more effective than that of $CaCO_3$. Therefore, even small amounts of Mg^{2+} can compete effectively for adsorption positions on the surfaces. Mg^{2+} can promote nucleation of calcite on stainless steel and thus shorten the induction time but still not promote further growth of crystals. It would be important that nucleation is avoided. Secondly, inhibition of further growth of already nucleated crystals is beneficial but it does not prevent fouling. Findings in this paper show that Mg^{2+} has important role on the nucleation and morphology of the calcite crystals in their further growth. When designing new non-fouling surfaces or inhibiting crystal growth in order to mitigate fouling, the impurity ions (also other than Mg^{2+}) are beneficial to take into account.

ACKNOWLEDGEMENTS

NOMENCLATURE

BFDH   Bravais-Friedel Donnay-Harker method
CASTEP   CAmbridge Serial Total Energy Package
DLC   Diamond Like Carbon
GGA-PBE   Perdew, Burke and Ernzerhof version of generalized gradient approximation functional
GGA-RPBE   Hammer, Hansen, Norskov modified Perdew, Burke and Ernzerhof version of generalized gradient approximation
PVD   Physical Vapour Deposition
PECVD   Plasma Enhanced chemical vapour deposition
SEM   scanning electron microscopy
XRD   X-Ray Diffraction

REFERENCES

Accelrys, 2004, MS Modeling, Release 3.1. San Diego:Accelrys Software Inc.

Accelrys, 2006, *MS Modeling*, Release 4.1. San Diego: Accelrys Software Inc.

Accelrys, 2007, *MS Modeling*, Release 4.2. San Diego: Accelrys Software Inc.

Accelrys, 2008a, *MS Modeling*, Release 4.3. San Diego: Accelrys Software Inc.

Accelrys, 2008b, *MS Modeling*, Release 4.3.1. San Diego: Accelrys Software Inc.

Accelrys, 2009, *MS Modeling*, Release 5.0. San Diego: Accelrys Software Inc.

Andritsos, N., and Karabelas, A. J., 2003, Calcium carbonate scaling in a plate heat exchanger in the precence of particles, *Int. J. Heat Mass Transfer*, Vol. 46, pp. 4613-4627.

Astilleros, J. M., Fernández-Díaz, L., and Putnis, A,. 2010, The role of magnesium in the growth of calcite: An AFM study, Chemical Geology, Vol. 271, pp. 52–58.

Bott, T. R., 1995, *Fouling of Heat Exchangers*, Elsevier, Amsterdam.

Bott, T. R., 1997, Aspects of Crystallization Fouling, *Experimental Thermal and Fluid Science*, Vol. 14, p. 356.

Cappus, D., Ehrlich, C. X. D., Dillmann, B., Ventrice, C. A. Jr., Shamery, K. A., Kuhlenbeck, H., and Freund, H.-J., 1993, Hydroxyl groups on oxide surfaces: NiO(100), NiO(111) and Cr_2O_3(111), *Chem. Phys.*, Vol. 177, pp. 533–546.

Chen, T., Neville, A., and Yuan, M., 2005, Assessing the effect of Mg^{2+} on $CaCO_3$ scale formation–bulk precipitation and surface deposition, *J. Crystal Growth*, Vol. 272, pp. e1341–e1347.

Chen, T., Neville, A., and Yuan, M., 2006, Influence of Mg^{2+} on $CaCO_3$ formation–bulk precipitation and surface deposition, *Chem. Eng. Sci.*, Vol. 61, pp. 5318–5327.

Grill, A., 1999, Diamond-like carbon: state of the art, *Diam. Relat. Mater.*, Vol. 8, pp. 428–434.

Henderson, M. A., and Chambers, S. A., 2000, HREELS, TPD and XPS study of the interaction of water with the α-Cr_2O_3(001) surface, *Surf. Sci.*, Vol. 449, pp. 135–150.

Henderson, M. A., 2002, The interaction of water with solid surfaces: fundamental aspects revisited, *Surf. Sci. Rep.*, Vol. 46, pp. 1–308.

Ignatchenko, A., Nealon, D. G., Dushane, R., and Humphries, K., 2006, Interaction of water with titania and zirconia surfaces, *J. Mol. Cat. A: Chem.*, Vol. 256, pp. 57–74.

Kostoglou, M., and Karabelas, A. J., 1998, Comprehensive Modeling of Precipitation and Fouling in Turbulent Pipe Flow, *Ind. Eng. Chem. Res.*, Vol. 37, pp. 1536–1550.

Laikhtman, A., Lafosse, A., Coat, Y. L., Azria, R., and Hoffman A., 2004, Interaction of water vapor with bare and hydrogenated diamond film surfaces, *Surf. Sci.*, Vol. 551, pp. 99–105.

Leach, A. R., 2001, *Molecular Modelling, Principles and Applications*, 2nd ed., Pearson Education Limited, Essex.

Macadam, J., and Parsons, S. A., 2004, Calcium carbonate scale control, effect of material and inhibitors, *Water Science and Technology*, Vol. 49, pp. 153-159.

Maurice, V., Cadot, S., and Marcus, P., 2001, Hydroxylation of ultra-thin films of α-Cr_2O_3 (0 0 0 1) formed on Cr (1 1 0), *Surf. Sci.*, Vol. 471, pp. 43–58.

Milošev, I., Strehblow, H.-H., and Navinšek, B., 1997, Comparison of TiN, ZrN and CrN hard nitride coatings: Electrochemical and thermal oxidation, *Thin Solid Films*, Vol. 303, pp. 246-254.

Müller-Steinhagen, H., 2002, *Heat Exchanger Fouling – Fundamental Approaches and Technical Solutions*, Publico Publications, Essen. p, XI.

Mwaba, M. G., Golriz, M. R., and Gu, J., 2006, A semi-empirical correlation for crystallization fouling on heat exchange surfaces, *App. Therm. Eng.*, Vol. 26, pp. 440–447.

Nishino, Y., Oaki, Y., and Imai, H., 2009, Magnesium-Mediated Nanocrystalline Mosaics of Calcite, *Cryst. Growth Des.*, Vol. 9, pp. 223–226.

Pießlinger-Schweiger, S., 2005, Surface treatment of metallic heat exchangers, *Heat Exchanger Fouling and Cleaning - Challenges and Opportunities*, Kloster Irsee, Germany, June 5 – 10, 2005, Engineering Conferences International, Brooklyn, NY, USA.

Puhakka, E., Riihimäki, M., and Keiski, R. L., 2008, Fouling mechanisms by *ab initio* calculations – Condensation reactions on the rutile (101) surface and adsorption of ions on the Cr_2O_3 surfaces, *Proceedings of the 7th International Conference on Heat Exchanger Fouling and Cleaning – Challenges and Opportunities*, eds. H. Müller-Steinhagen, M. R. Malayeri, and A. P. Watkinson, ECI Symposium series, Tomar, Portugal, July 1–6, 2007, The Berkeley Electronic Press, Vol. RP5, pp. 300–307.

Puhakka, E., Riihimäki, M., and Keiski, R., 2010, Structural design of surface materials in mitigation of fouling - Induction of crystal growth, *Extended Abstracts - Book B, First International Conference on Materials for Energy*, Karlsruhe, Germany, July 4-8, 2010. DECHEMA e.V., Frankfurt am Main, Germany, pp. 997-999.

Puhakka, E., Riihimäki, M., Pääkkönen, T., and Keiski, R. L., 2011, Density Functional Theory Studies on the Formation of $CaCO_3$ Depositions on Cristobalite, Diamond, and Titanium Carbide surfaces, *Heat Transfer Eng.*, Vol. 32, pp. 282–290.

Pääkkönen, T. M., Riihimäki, M., Puhakka, E., Muurinen, E., Simonson, C. J., and Keiski, R. L., 2010, Crystallization fouling of $CaCO_3$ – Effect of bulk precipitation on mass deposition on the heat transfer surface, *Proceedings of 8th International Conference on Heat Exchanger Fouling and Cleaning – 2009 (Peer-reviewed)*, eds. H. Müller-Steinhagen, M. R. Malayeri, and A. P. Watkinson, EUROTHERM Seminar No. 86 on Heat Exchanger Fouling and Cleaning – 2009, Schladming, Austria, June 14–19, 2009, EUROTHERM, pp. 209–216.

Riihimäki, M., Ojaniemi, U., Pättikangas, T. J. H., Pääkkönen, T. M., Manninen, M., Puhakka, E., Muurinen, E., Simonson, C. J., and Keiski, R. L., 2010, Fouling in high solid content suspension – Effect of nucleating air and background electrolyte, *Proceedings of 8th International Conference on Heat Exchanger Fouling and Cleaning – 2009 (Peer-reviewed)*, eds. H. Müller-Steinhagen, M. R. Malayeri, and A. P. Watkinson, EUROTHERM Seminar No. 86 on Heat Exchanger Fouling and Cleaning – 2009, Schladming, Austria, June 14–19, 2009, EUROTHERM, pp. 192–199.

Saunders, S. R. J., Monteiro, M., and Rizzo, F., 2008, The oxidation behaviour of metals and alloys at high temperatures in atmospheres containing water vapour: A review, *Prog. Mater. Sci.*, Vol. 53, pp. 775–837.

Yang, Q., Ding, J., and Shen, Z., 2000, Investigation on fouling behaviors of low-energy surface and fouling fractal characteristics, *Chem. Eng. Sci.*, Vol. 55, pp 797-805.

Yang, Q., Liu, Y., Gu, A., Ding, J., and Shen, Z., 2002, Investigation of induction period and morphology of $CaCO_3$ fouling heated surface, *Chem. Eng. Sci.*, Vol. 57, pp. 921-931.